

Preparation and Characterisation of Battery-grade $\text{Na}_2\text{Mn}_3\text{O}_7$ as a Cathode Material from Manganese Ore

Yolanda Escobar-Martínez¹, Elsa Arce-Estrada¹, Antonio Romero-Serrano^{1,*}, Aurelio Hernández-Ramírez¹, Josué López-Rodríguez¹, Alejandro Cruz-Ramírez² and Enrique Rivera-Salinas³

¹ Instituto Politécnico Nacional, ESIQIE, Metallurgy and Materials, Ciudad de Mexico, Mexico.

² Instituto Politécnico Nacional- UPIIH. Hidalgo, Mexico

³ Consejo Nacional de Ciencia y Tecnología (CONACyT) – Departamento de Procesos de Transformación, Centro de Investigación en Química Aplicada (CIQAA), Saltillo, Mexico.

*E-mail: romeroipn@hotmail.com

Received: 19 March 2021 / Accepted: 4 May 2021 / Published: 31 May 2021

Natural battery-grade manganese dioxide with 69.78 mass% MnO_2 and 14.50% MnCO_3 was subjected to solid-state treatment to prepare a hybrid system with $\beta\text{-MnO}_2$ and $\text{Na}_2\text{Mn}_3\text{O}_7$ phases. The heat treatment was carried out at 400°C using NaOH/MnO_2 molar ratios ranging 0.4 to 1.2 and $\text{NaNO}_3/\text{MnO}_2$ molar ratios ranging 0 to 0.8. The structures of the samples were analysed using X-ray diffraction and differential scanning calorimetry. The electrochemical properties were evaluated through cyclic voltammetry, and the specific capacitance (C_s) values were calculated. The XRD results confirmed the formation of $\text{Na}_2\text{Mn}_3\text{O}_7$. The highest C_s (34.21 F g⁻¹) was obtained in the sample with 24.15 mass% $\text{Na}_2\text{Mn}_3\text{O}_7$. A thermodynamic analysis was also carried out to estimate the effect of the NaOH and NaNO_3 contents and of the temperature on the formation of Mn-based species.

Keywords: solid state treatment; $\text{Na}_2\text{Mn}_3\text{O}_7$ species; specific capacitance.

1. INTRODUCTION

In recent years, $\text{Na}_x\text{M}_y\text{O}_z$ ($\text{M} = \text{Mn, Ni, Co}$) materials have been considered possible supplements to lithium-ion batteries due to the abundance of sodium and the low cost of the material [1,2]. Among these cathode materials, $\text{Na}_x\text{M}_y\text{O}_z$ species are considered promising due to their theoretically high capacity, ease of synthesis and environmentally friendly nature. Various $\text{Na}_x\text{M}_y\text{O}_z$ materials have been successfully prepared by several methods, such as solid-state [3-6], hydrothermal [7,8], sol-gel [9,10] and molten salt synthesis procedures [11].

Matsumae [12] prepared sodium manganese oxide, including $\alpha\text{-NaMnO}_2$, $\beta\text{-NaMnO}_2$ and $\text{Na}_{0.7}\text{MnO}_2$, as a cathode material for sodium-ion secondary batteries by a microwave heating method

with a boron addition. Manzi [13] reported a physico-chemical comparison of α - and β -NaMnO₂ compounds as materials for application in electrodes for secondary sodium batteries. Tsuchimoto [14] reported that Na_{2-x}Mn₃O₇ electrodes had a highly reversible oxygen-redox capacity with small polarization using spectroscopic and magnetic measurements. Whitacre [15] prepared Na₄Mn₉O₁₈ by a solid-state synthesis route combining Na₂CO₃ and Mn₂O₃ at 750–800°C for 8 h and found that the system was electrochemically stable in an aqueous 1 M Na₂SO₄ electrolyte. Marlina [16] synthesized Na₂Mn₃O₇ by mixing Na₂CO₃ and MnO₂ in a solid state method and by mixing Na₂CO₃ and MnCl₂ by a sol-gel method, followed by calcination at 800°C for 3 h.

Low grade manganese ore has been used to prepare MnO₂ materials, where it is first reduced to MnO. Then, soluble MnO is leached by dilute sulfuric acid to obtain a MnSO₄ solution, and finally, structural MnO₂ can be prepared by the redox reaction in a mixed solution of MnSO₄ and KMnO₄ [17]. Zhao [18] chemically prepared manganese dioxide from low-grade rhodochrosite (MnCO₃) ore by leaching with sulfuric acid, purifying, crystallising and decomposing MnCO₃, before finally refining MnO₂. These leaching methods decrease the contents of ore impurities such as silica and iron oxides.

In the present work it is proposed to prepare a hybrid mixture of β -MnO₂ and Na₂Mn₃O₇ components from natural battery-grade manganese dioxide, which is used in the manufacture of dry-cell batteries, to improve the specific capacitance of this material. The manganese ore concentrate contains pyrolusite (β -MnO₂) and rhodochrosite (MnCO₃) in a mass ratio of 4.8/1 (MnO₂/MnCO₃), along with small amounts of silica, corundum, iron oxide and CaO. The solid state treatment partially transforms MnO₂ and MnCO₃ into Na₂Mn₃O₇ by reacting with NaOH and the oxidant agent NaNO₃, at 400°C in a controlled atmosphere. The chemical composition and microstructure of the Na₂Mn₃O₇ samples are examined by chemical analysis, X-ray diffraction (XRD) and differential scanning calorimetry (DSC). The electrochemical properties of the Mn-based materials are investigated by cyclic voltammetry (CV), and on the basis of the CV data, the specific capacitance values are calculated. A thermodynamic analysis is also carried out with FACTSage software [19] to estimate the effect of the content of NaOH and NaNO₃ and of the temperature on the thermodynamic stability of the different Mn-based compounds.

2. EXPERIMENTAL

The experimental design was based on the composition of the manganese ore concentrate, which mainly contains pyrolusite (β -MnO₂) and rhodochrosite, as shown in Table 1 (moisture was excluded).

Table 1. Chemical composition of the manganese ore concentrate. n_i/n_{MnO₂} represents the ratio of the moles of each component to the moles of MnO₂.

Component	mass%	n _i /n _{MnO₂}
MnO ₂	69.78	1
MnCO ₃	14.50	0.1570
SiO ₂	6.85	0.1420
Al ₂ O ₃	3.50	0.0427
Fe ₂ O ₃	3.27	0.0255
CaO	2.1	0.0466

The particle size of the manganese ore was lower than 74 μm (< mesh 200). The ore concentrate was characterised by X-ray diffraction, scanning calorimetry and chemical analysis. Subsequently, the solid state treatment of the manganese ore samples was carried out using NaOH and NaNO₃ at different NaOH/MnO₂ and NaNO₃/MnO₂ molar ratios, as shown in Table 2.

Table 2. Experimentally used molar ratios of NaOH and NaNO₃.

Sample	n _{NaOH} /n _{MnO₂}	n _{NaNO₃} /n _{MnO₂}
A-1	0.4	0
A-2	0.4	0.4
A-3	0.4	0.8
B-1	0.8	0
B-2	0.8	0.4
B-3	0.8	0.8
C-1	1.2	0
C-2	1.2	0.4
C-3	1.2	0.8

Chemically pure NaOH and NaNO₃ powders (above 99.5 mass% purity) were homogeneously mixed with manganese ore, placed in a nickel crucible and heated in an alumina tube furnace with an argon atmosphere. The samples were heated to 400°C and kept at this temperature for four hours in order to reach equilibrium. The temperature was measured with an R-type thermocouple (Pt - Pt, 13% Rh). The samples were cooled to room temperature and the reaction product was washed with a dilute acidic HCl solution to remove water-soluble salts and thereby obtain a solid product that was enriched with Na₂Mn₃O₇. Then, the samples were prepared for characterisation by X-ray diffraction (Bruker AXS diffractometer model D8, equipped with a Cu K α radiation source), differential scanning thermal analysis (Mettler Toledo TGA-DSC-1) and chemical analysis.

The electrochemical evaluation of the synthesized materials was performed by means of the cyclic voltammetry technique using an EG&G potentiostat/galvanostat (Princeton Applied Research, model 273A). A typical 3-electrode electrochemical cell consisting of a saturated calomel reference electrode, ECS ($E^\circ = 0.2415 \text{ V/ENH}$) placed inside a Luggin capillary, a graphite counter electrode and a working electrode. The working electrode was prepared using 0.0004 g of Vulcan carbon, 10 μl of Nafion and 60 μl of acetone. Cyclic voltammetry measurements were carried out at a scan rate of 2 mV s^{-1} over the voltage range of -0.9 to 0.4 V. The specific capacitance (C_S) values of the electrode materials were also calculated from the voltammetry results.

3. THERMODYNAMIC ANALYSIS

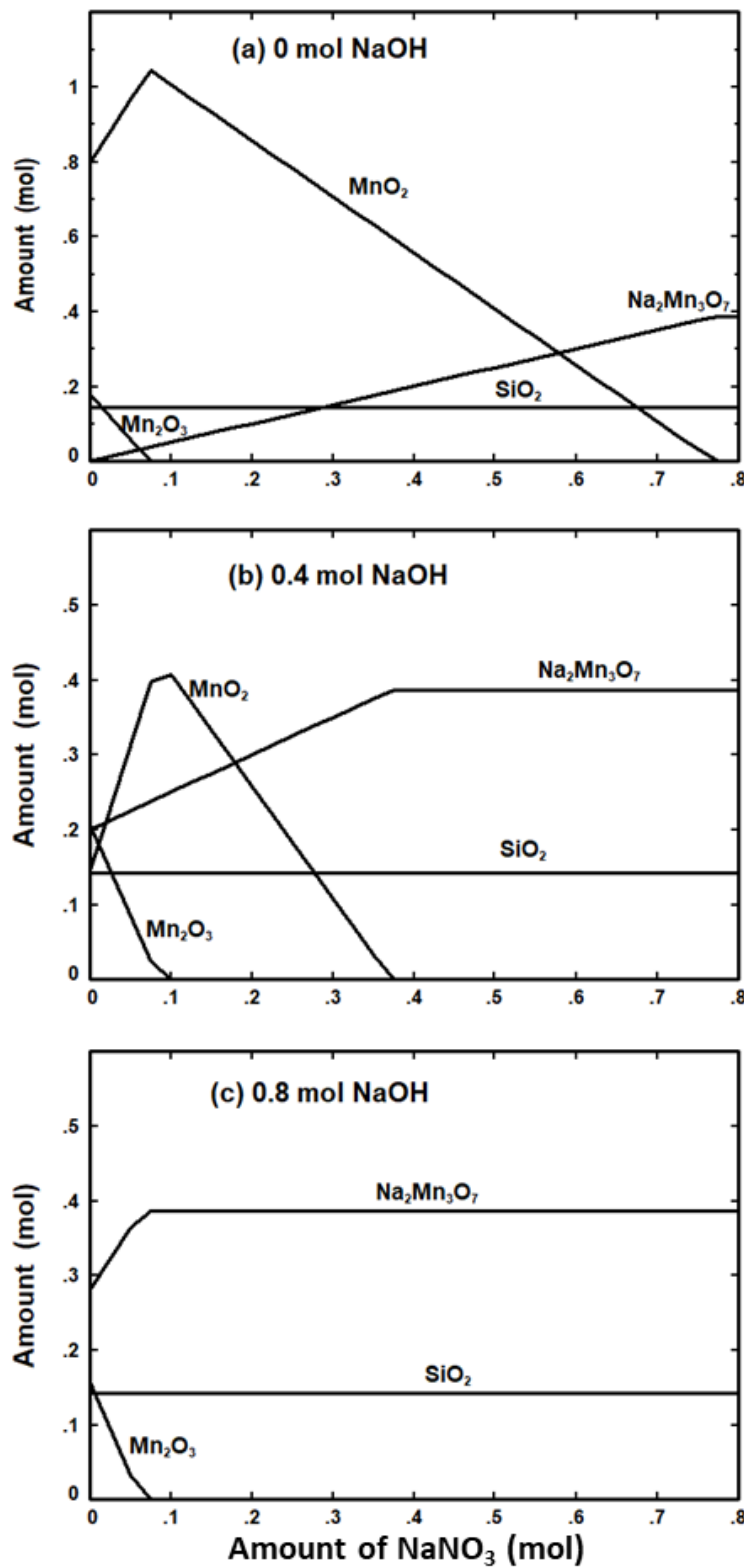


Figure 1. Effect of the amounts of NaOH and NaNO_3 on the amounts of Mn-based compounds at 400°C.

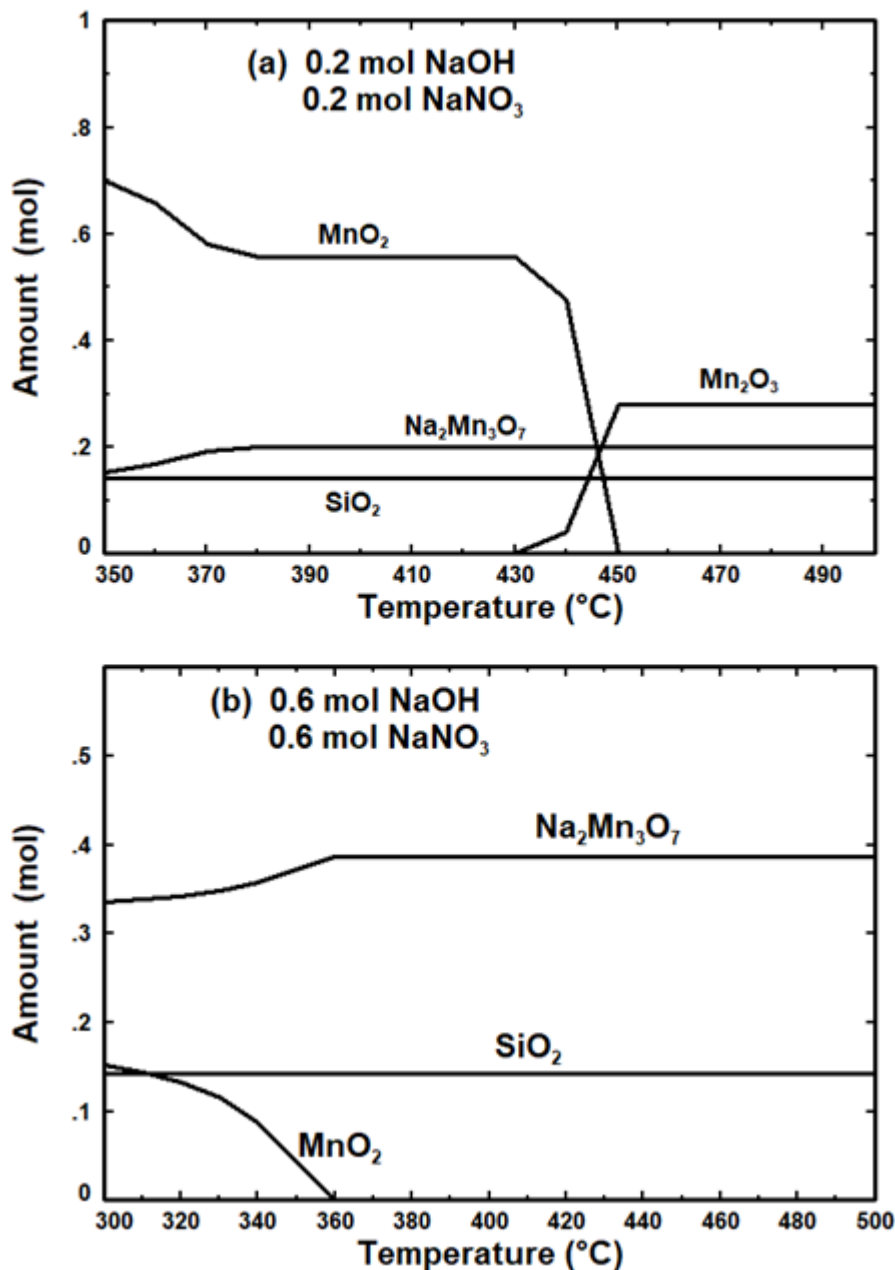


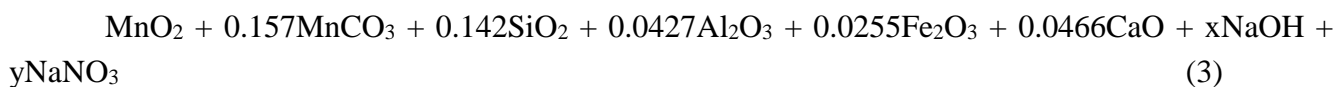
Figure 2. Effect of temperature on the amounts of the Mn-based compounds.

The FACTSage computational thermodynamic package [19] with the Equilib module was used to determine the concentration of the different chemical species once they reached chemical equilibrium. The user provides the initial amounts of the chemical species contained in the system along with the temperature and pressure. Then, the program calculates the most stable species with the Gibbs free energy minimisation method. It is worth mentioning here that to complete the FACTSage database, we included the molar enthalpy (H°_{298}) and molar entropy (S°_{298}) of Na₂Mn₃O₇ at 298.15 K which was estimated by the methods reported by Aronson [20] and Spencer [21], respectively. The Neumann-Kopp Rule [22] was applied to calculate the standard molar heat capacity of Na₂Mn₃O₇, C_p° , from the contribution of the heat capacity of the oxides Na₂O and MnO₂:

$$H^\circ_{298} = -2,120.0 \text{ kJ mol}^{-1} ; S^\circ_{298} = 273.30 \text{ J mol}^{-1} \text{ K}^{-1} \quad (1)$$

$$C_p^\circ = 278.721 + 0.0667 T - 5.7964 \times 10^6 T^{-2} - 14.088 \times 10^{-6} T^2 \text{ J mol}^{-1} \text{ K}^{-1} \quad (2)$$

To estimate the effects of the NaOH and NaNO₃ contents and of the temperature, the molar amounts of each component, shown in Tables 1 and 2, were considered in the FACTSage software, which can be expressed as:



where x and y are considered to be between 0 and 0.8.

Figure 1 shows the calculated composition of the chemical species in terms of the content of NaOH and NaNO₃ at 400°C, where it is observed that the combined effect of these fluxes can produce a complete transformation of MnO₂ and MnCO₃ to Na₂Mn₃O₇. As the alkali hydroxide to manganese dioxide ratio is increased, the yield of higher valence materials also increases. In addition, the presence of the oxidising agent (NaNO₃) prevents the formation of Mn₂O₃. According to the thermodynamic calculation, the minor components SiO₂, Al₂O₃, CaO and Fe₂O₃ do not react at this temperature; thus, not all of them are shown in Figure 1. Figure 2 shows that the processing temperature is important to avoid the formation of Mn₂O₃ and to obtain the highest content of Na₂Mn₃O₇, which depends on the contents of NaOH and NaNO₃.

4. RESULTS AND DISCUSSION

4.1 Chemical analysis

Flame emission spectroscopy (FES) was used for the determination of Na in the heat treated manganese ore. The Na content was considered to completely form the Na₂Mn₃O₇ component. Table 3 shows the Na content, and hence the obtained Na₂Mn₃O₇ amount in each sample. It is observed that by increasing the contents of both NaOH and NaNO₃ in the treatments the sodium content also increases. The highest Na₂Mn₃O₇ amount is obtained in sample C-3, which is treated with the following molar ratios, NaOH/MnO₂ = 1.2 and NaNO₃/MnO₂ = 0.8.

Table 3. Chemical composition and specific capacitance of the heat treated samples.

Sample	mass% Na	mass% Na ₂ Mn ₃ O ₇	Cs (F g ⁻¹)
A-1	1.3	9.13	13.78
A-2	1.7	11.93	15.70
A-3	2.6	18.25	24.31
B-1	1.62	11.37	16.04
B-2	2.0	14.04	19.12
B-3	2.90	20.36	27.50
C-1	2.46	17.27	25.18
C-2	3.15	22.11	30.13
C-3	3.44	24.15	34.21

The initial MnCO_3 content of the ore concentrate (14.5 mass%) should provide 13.57 mass% $\text{Na}_2\text{Mn}_3\text{O}_7$, if assuming complete transformation; however, some samples have less than this value, as shown in Table 3. This result means that in these samples, rhodochrosite is partially transformed into pyrolusite. Thus, the heat-treated samples can be considered a hybrid system consisting of $\beta\text{-MnO}_2$ and $\text{Na}_2\text{Mn}_3\text{O}_7$.

4.2 DSC results

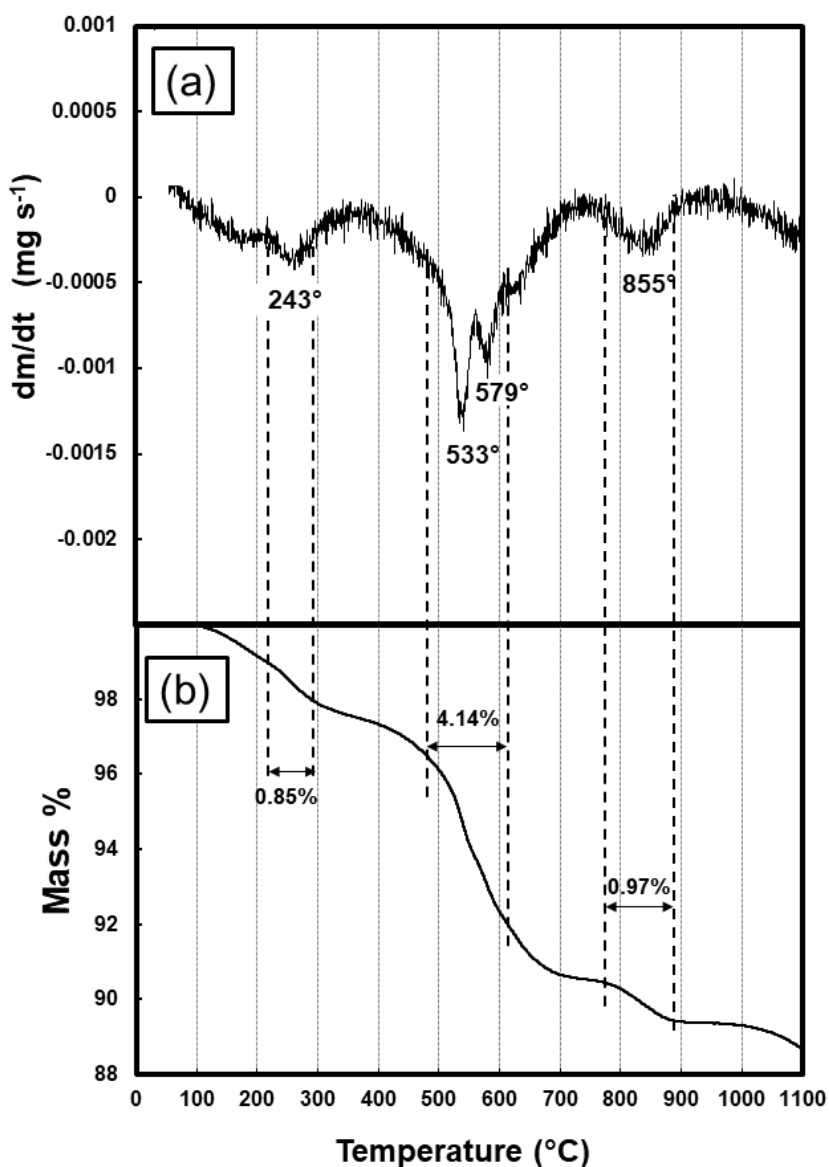


Figure 3. DSC pattern of the manganese ore concentrate.

Figure 3 shows the DSC pattern of the initial manganese ore concentrate. The resolution of the individual steps in the DSC curves can be improved by examining the derivative curves (Figure 3.a) which represents the rate of mass loss; the peaks more accurately indicate the specific temperatures characteristic of the different component changes.

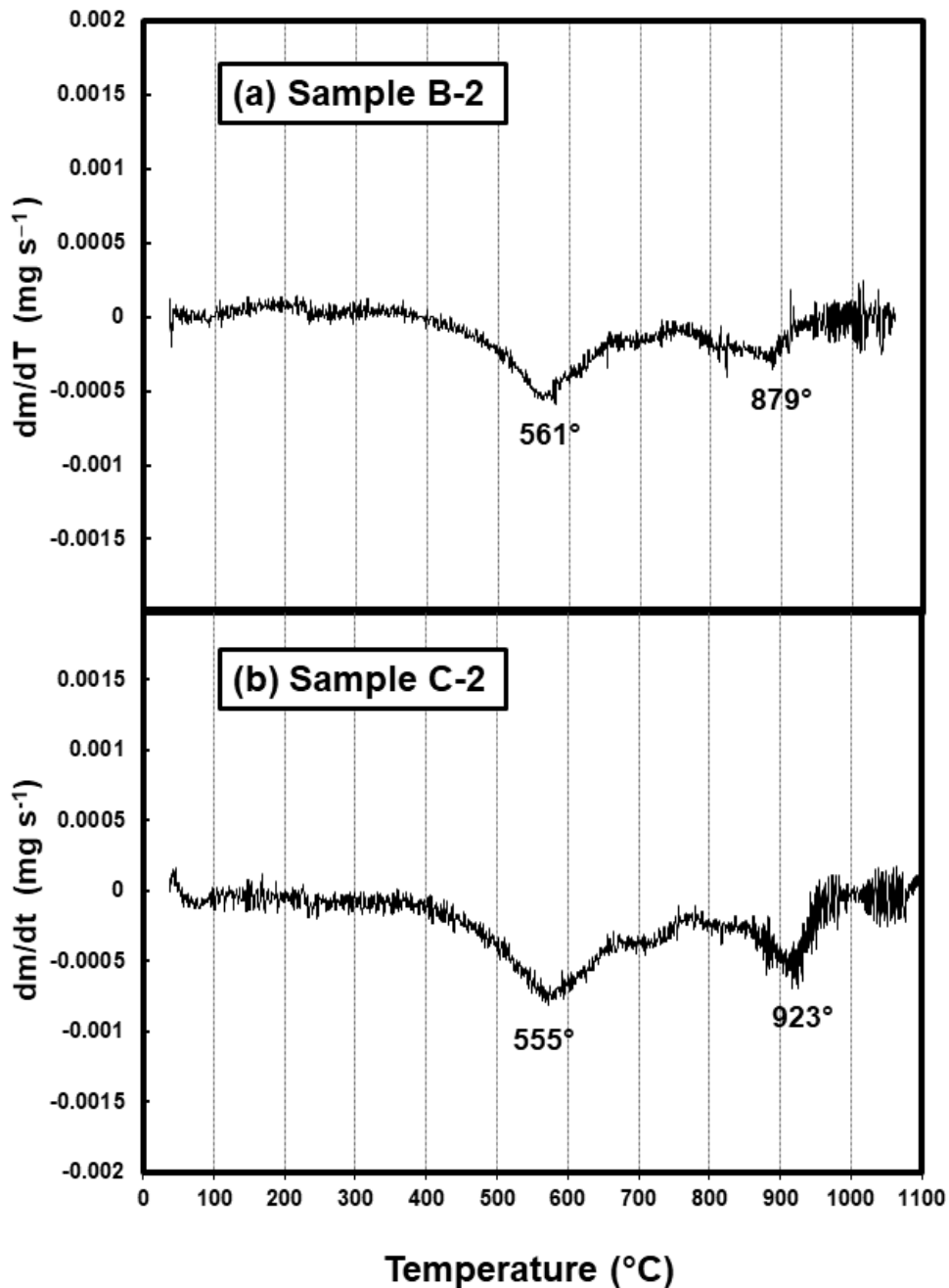


Figure 4 DSC patterns of the samples treated with molar ratios of (a) $\text{NaNO}_3/\text{MnO}_2=0.4$ and $\text{NaOH}/\text{MnO}_2=0.8$ and (b) $\text{NaNO}_3/\text{MnO}_2=0.4$ and $\text{NaOH}/\text{MnO}_2=1.2$.

This figure shows an endothermic peak at approximately 243°C with 0.85% weight loss, which may be ascribed to the removal of structural water [23,24], and an endothermic decomposition reaction of rhodochrosite between 480° and 630°C [23]:



This reaction immediately overlaps the reduction (Mn^{4+} to Mn^{3+}) and oxidation (Mn^{2+} to Mn^{3+}) reactions:



An endothermic reduction takes place at approximately 855°C:

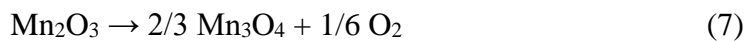


Figure 3.b shows that the mass loss during reactions (4) to (6) was approximately 4.14%, whereas the mass loss during reaction (7) was approximately 0.97%.

Figure 4 shows the DSC patterns of samples B-2 and C-2 after the solid state treatment of the ore concentrate. There is no peak for the rhodochrosite transformation at approximately 533°C, which means that this component is completely transformed, first to MnO and then to MnO₂ or Na₂Mn₃O₇. There is a small peak between 550° and 570°C for the MnO₂→Mn₂O₃ transformation, and one peak between 879° and 923°C for the Mn₂O₃→Mn₃O₄ transformation. Similar DSC patterns are obtained for the other samples.

4.3 Structure of the heat treated manganese ore

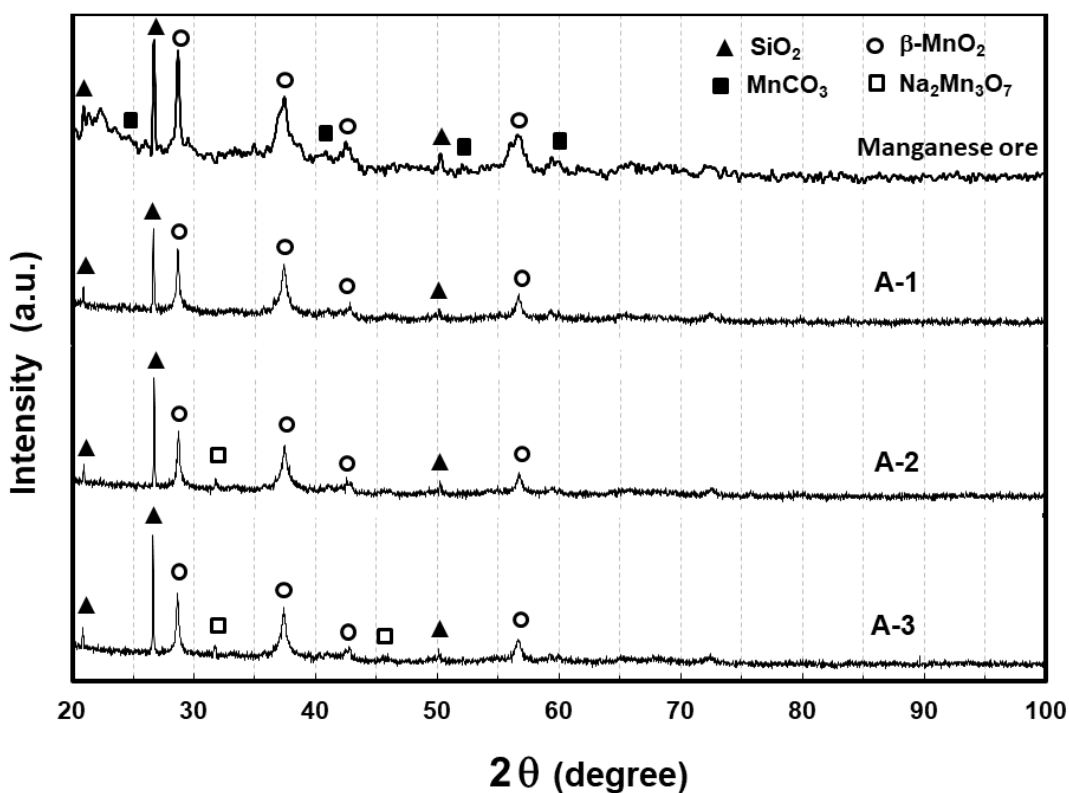


Figure 5. XRD patterns of the samples treated with molar ratio of NaOH/MnO₂=0.4.

The powder XRD patterns of the manganese ore concentrate as well as the samples heat treated with a molar ratio of NaOH/MnO₂ = 0.4 are shown in Figure 5. There are four peaks at approximately $2\theta = 28.62^\circ$, 37.37° , 42.79° and 56.57° , which demonstrate the presence of pyrolusite $\beta\text{-MnO}_2$ (JCPDS No. 24-735). The peaks of rhodochrosite (JCPDS No. 44-1472) and quartz-SiO₂ (JCPDS No. 78-1254) can also be observed. Small peaks at approximately 32.13° and 45.35° are observed in samples A-2

and A-3 which correspond to the $\text{Na}_2\text{Mn}_3\text{O}_7$ species (JCPDS No. 78-0193), whereas the peaks of MnCO_3 cannot be observed in these samples.

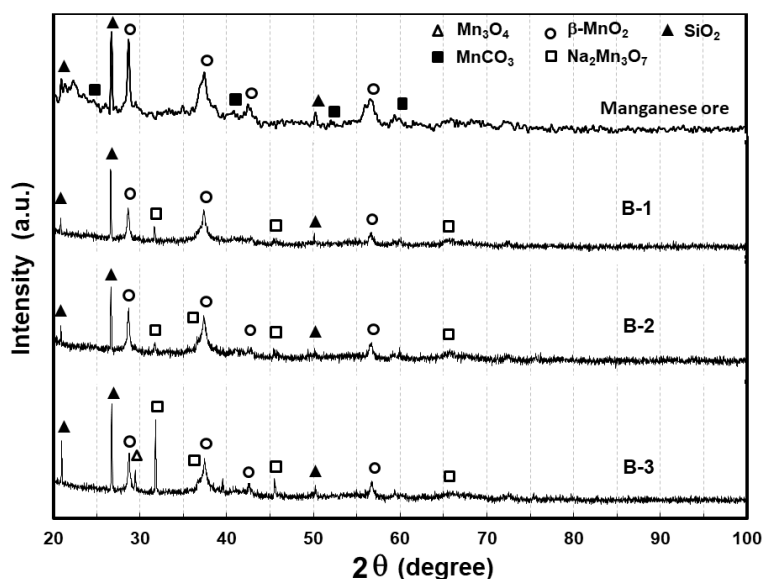


Figure 6. XRD patterns of the samples treated with molar ratio of $\text{NaOH}/\text{MnO}_2=0.8$.

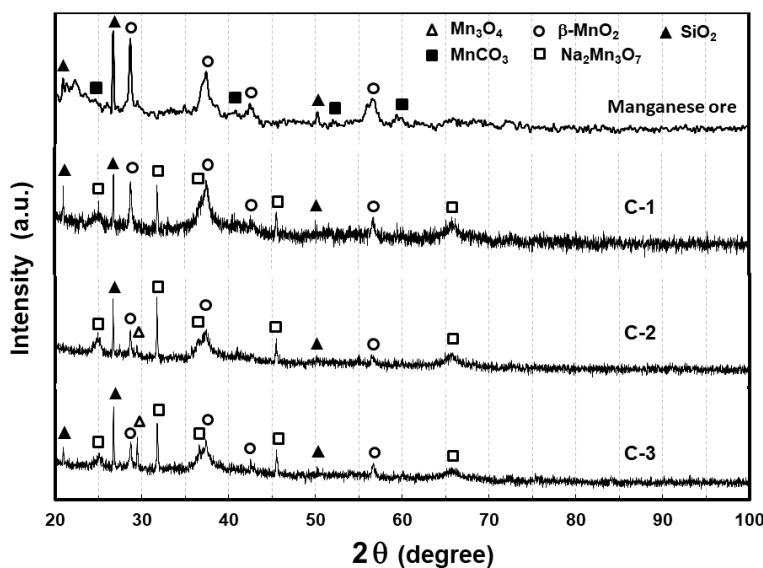


Figure 7. XRD patterns of the samples treated with molar ratio of $\text{NaOH}/\text{MnO}_2=1.2$.

Figures 6 and 7 show the XRD patterns for the samples treated with $\text{NaOH}/\text{MnO}_2 = 0.8$ and 1.2, respectively. In these samples the peaks at 24.97° , 32.13° , 36.18° , 45.35 and 65.31° corresponding to $\text{Na}_2\text{Mn}_3\text{O}_7$ are more clearly observed, especially for the samples obtained with high $\text{NaNO}_3/\text{MnO}_2$ molar ratios (B-3 and C-3), this result corresponds with the highest amount of $\text{Na}_2\text{Mn}_3\text{O}_7$ obtained in these samples.

It has been reported that $\text{Na}_2\text{Mn}_3\text{O}_7$ is obtained by solid methods from NaNO_3 and MnCO_3 ; thus, the structure of the as-synthesized materials was analysed by using high-resolution X-ray diffraction [25,26]. Stoichiometric amounts of the precursors were used in these works to completely obtain $\text{Na}_2\text{Mn}_3\text{O}_7$.

4.4 Electrochemical performance of the heat treated samples

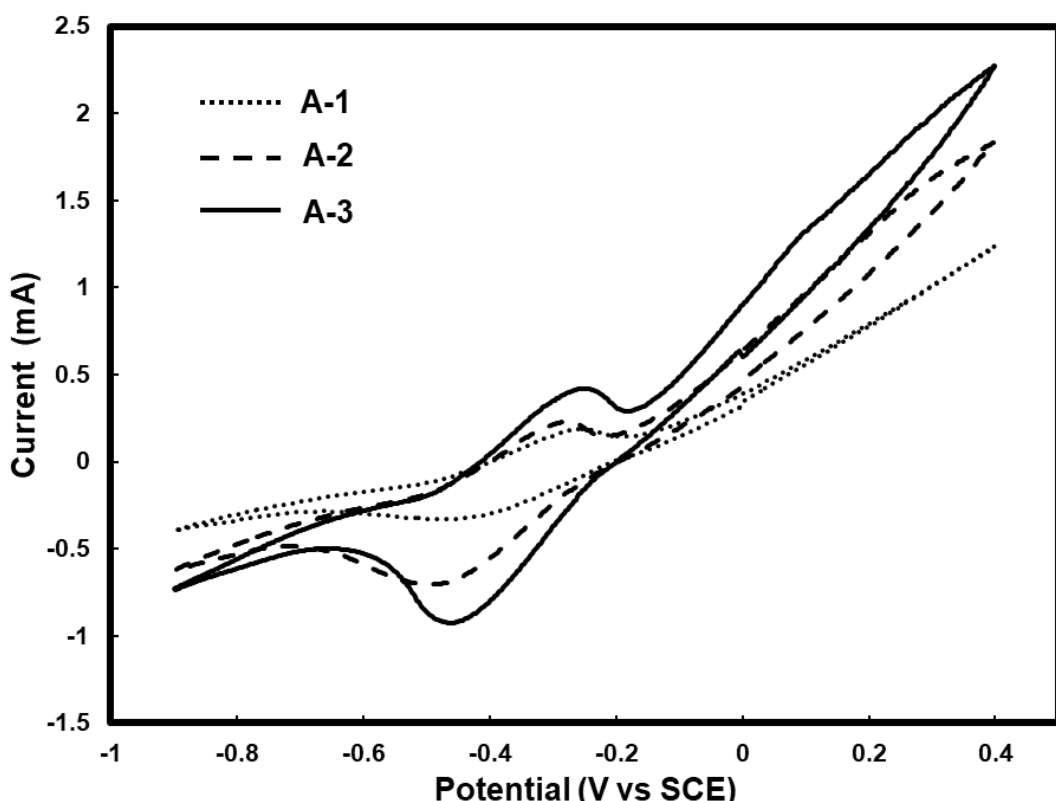


Figure 8. CV curves of the samples treated with a molar ratio of $\text{NaOH}/\text{MnO}_2=0.4$.

The electrochemical properties of the heat treated manganese ore specimens were determined by cyclic voltammetry at room temperature. Figure 8 shows the measured CV curves of samples A-1, A-2 and A-3 recorded at a scan rate of 2 mV s^{-1} and between -0.9 and $+0.4 \text{ V}$ vs. Hg/HgO in a three-electrode cell with activated carbon. The presence of a pair of redox peaks is observed, corresponding to the charge/discharge plateaus of the voltage curves. Specifically, in the cathodic sweep of these three samples, at approximately -0.5 to -0.4 V vs. Hg/HgO , current peaks are observed which are due to the reduction of Mn^{4+} accompanying the insertion of Na^+ ions. In the reverse direction, oxidation peaks are observed between -0.3 and -0.2 V vs. Hg/HgO , which are due to the removal of Na^+ ions. Thus, the capacitance originates from the fast and reversible Faradaic redox mechanism [27].

The redox peaks of these samples are similar in position and shape, which indicates that the charge storage mechanisms of these materials are the same. However, the anodic peak increases as the Na content in the heat-treated sample increases.

Generally, the oxidation peak and reduction peak move towards high potential and low potential, respectively, indicating slow ion diffusion, higher diffusion resistance and polarisation within the electrode material [28]. However, the treated manganese ore samples show that there are small potential differences between the cathodic and anodic peaks (less than 0.2 V), suggesting little polarization and fast electrode kinetics.

The specific capacitance was calculated from the CV curves using the following equation:

$$C_s = \frac{Q}{\Delta V} = \frac{1}{v m \Delta V} \int_{V_a}^{V_c} I dV \quad (8)$$

where C_s ($F g^{-1}$) is the specific capacitance, Q ($C g^{-1}$) represents the voltammetric charge obtained from the integrated area of the CV curves, v is the potential scan rate ($V s^{-1}$), $\Delta V = (V_c - V_a)$ is the sweep potential range (V), I denotes the response current (A), and m is the mass of the electroactive material (g).

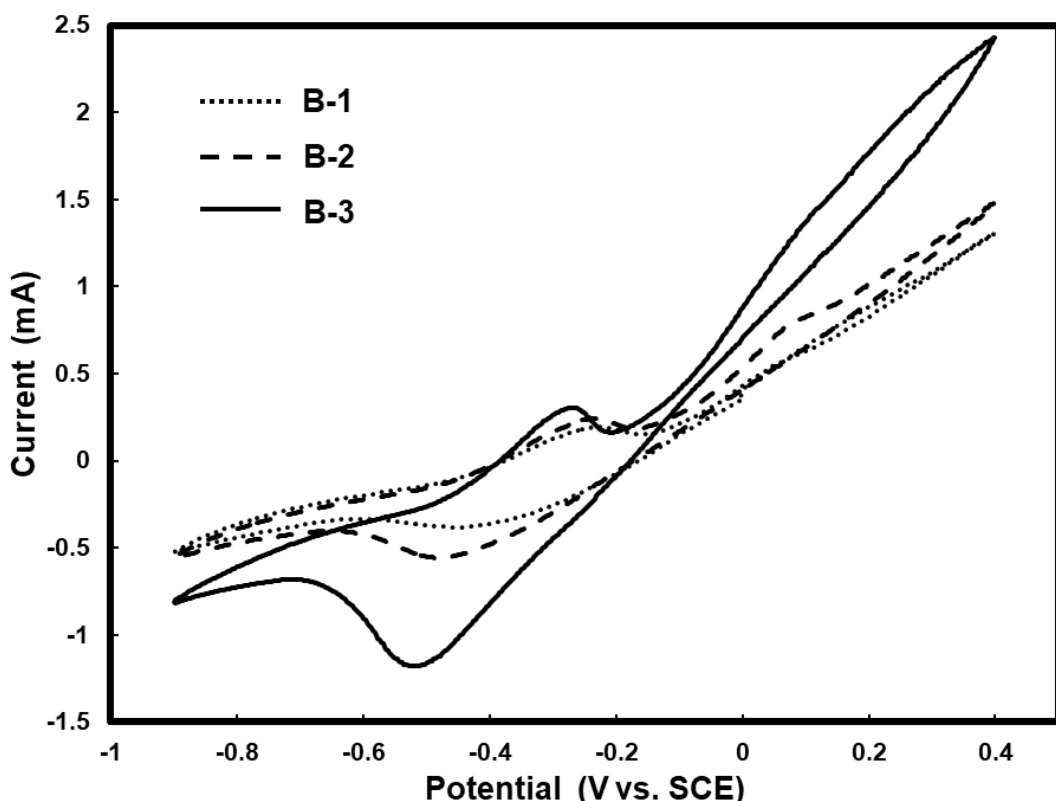


Figure 9. CV curves of the samples treated with a molar ratio of $NaOH/MnO_2=0.8$.

The specific capacitance values of samples A-1, A-2 and A-3, calculated from the CV curves and reported in Table 3, are 13.78 , 15.7 and $24.31 F g^{-1}$, respectively. The specific capacitance of sample A-3 is higher than that of A-1 and A-2. This result can be due to the content of $Na_2Mn_3O_7$ being highest in the tested electrode.

Figures 9 and 10 show the measured CV curves of samples for the B and C series of materials treated with molar ratios of $NaOH/MnO_2 = 0.8$ and 1.2 , respectively. A peak is observed in these samples during the cathodic sweep, corresponding to the reduction of Mn^{4+} and the insertion of Na^+

ions, and a peak during the anodic sweep corresponding to the removal of Na^+ ions. Again, it is observed that the samples with more $\text{Na}_2\text{Mn}_3\text{O}_7$ present a higher integrated area of the CV curves and consequently a larger specific capacitance. As reported in Table 3, the highest specific capacitance is 34.21 F g^{-1} , corresponding to sample C-3, which contains 3.44 mass%Na (24.15 mass% $\text{Na}_2\text{Mn}_3\text{O}_7$). Specific capacitance values from 13.78 to 34.21 F g^{-1} , as shown in Table 3, agree with values previously reported for the β - MnO_2 and $\text{Na}_2\text{Mn}_3\text{O}_7$ phases [14,29].

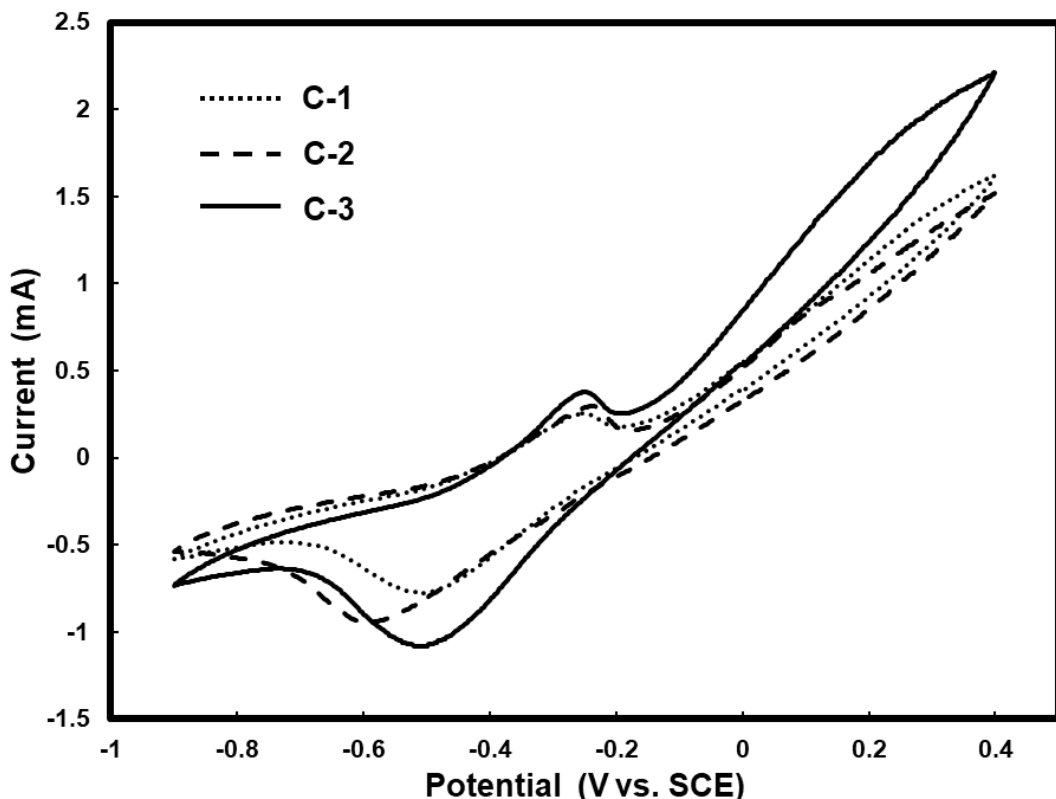


Figure 10. CV curves of the samples treated with a molar ratio of $\text{NaOH}/\text{MnO}_2=1.2$.

Pyrolusite has a very low specific capacitance [29], but we have shown in this work that the Cs of natural battery-grade manganese dioxide can be improved by a simple solid-state treatment through a partial transformation to $\text{Na}_2\text{Mn}_3\text{O}_7$, which has a higher Cs. The maximum $\text{Na}_2\text{Mn}_3\text{O}_7$ content obtained in this work is approximately 24 mass%, and further work is needed to increase this content by increasing the contents of NaOH and NaNO_3 in the solid-state treatment.

5. CONCLUSIONS

Natural battery-grade manganese dioxide was subjected to high-temperature solid-state treatment to prepare a hybrid mixture of β - MnO_2 and $\text{Na}_2\text{Mn}_3\text{O}_7$ species. XRD confirmed the formation of $\text{Na}_2\text{Mn}_3\text{O}_7$ at the treatment temperature (400°C), while the DSC results revealed that all the MnCO_3 was transformed into MnO_2 or $\text{Na}_2\text{Mn}_3\text{O}_7$. The combined effect of the NaOH and NaNO_3

contents and of the temperature increased the amount of $\text{Na}_2\text{Mn}_3\text{O}_7$ and prevented the formation of Mn_2O_3 . The Cs increased from 13.78 F g^{-1} to 34.21 F g^{-1} for the samples with 9.13 and 24.15 mass% $\text{Na}_2\text{Mn}_3\text{O}_7$, respectively. Therefore, we conclude that a higher Cs can be obtained by increasing the $\text{Na}_2\text{Mn}_3\text{O}_7$ content using this method, which may be attractive for use in energy storage devices.

ACKNOWLEDGMENTS

The authors wish to thank the National Council for Science and Technology (CONACYT), National Polytechnic Institute (IPN) and the Researcher National System (SNI) for the support of this research.

References

1. A. Eftekhari, D.W. Kim, *J Power Sources*, 395 (2018) 336.
2. Y. Zhang, R. Zhang and Y. Huang, *Front. Chem.*, 7 (2019) 335.
3. X. Ma, H. Chen and G. Ceder, *J Electrochem. Soc.*, 158 (2011) A1307.
4. J. Billaud, R.J. Clément, A.R. Armstrong, J. Canales-Vázquez, P. Rozier, C.P. Clare and P.G. Bruce, *J. Am. Chem. Soc.*, 136 (2014) 17243.
5. Y. Li, X. Feng, S. Cui, Q. Shi, L. Mi and W. Chena, *CrystEngComm*, 18 (2016) 3136.
6. M. Xu, Y. Niu, C. Chen, J. Song, S. Baoab and C.M. Li, *RSC Adv.*, 4 (2014) 38140.
7. R. Kataoka, M. Kitta, N. Takeichi, and T. Kiyobayashiz, *J Electrochem. Soc.*, 164 (2017) A226.
8. E. Hosonoaa, H. Matsudaa, I. Honmaa, S. Fujiharab, M. Ichiharac and H. Zhoua, *J Power Sources*, 182 (2008) 349.
9. M. H. Han, E. Gonzalo, G. Singha and T. Rojo, *Energy Environ. Sci.*, 8 (2015) 81.
10. X. Zhou, R.K. Guduru and P. Mohant, *J. Mater. Chem. A.*, 1 (2013) 2757.
11. L. Zhao, J. Ni, H. Wang and L. Gao, *Funct. Mater. Lett.*, 6 (2013) 1350012.
12. Y. Matsumae, R. Suzuki, K. Komiyai and M. Higuchi, *J. Ceram. Soc. Jpn.*, 128 (2020) 544.
13. J. Manzi, A. Paolone, O. Palumbo, D. Corona, A. Massaro, R. Cavaliere, A.B. Muñoz-García, F. Trequattrini, M. Pavone and S. Brutti, *Energies*, 14 (2021) 1230.
14. A. Tsuchimoto, X-M. Shi, K. Kawai, B. Mortemard de Boisse, J. Kikkawa, D. Asakura, M. Okubo and A. Yamada, *Nat Commun.*, 12 (2021) 631.
15. J.F. Whitacre, A. Tevar and S. Sharma, *Electrochim. Commun.*, 12 (2010) 463.
16. H. A. Marlina, K. Sebayang, S. Gea, Z. Noer, R. Septawendar and B. Sunendar, *J. Ceram. Soc. Jpn.*, 128 (2020) 970.
17. Y. Zhao and G. Zhu, *MOJ App. Bio. Biomech.*, 2 (2018) 57.
18. J. Zhao, L. Xu and C. Xie, *Chin. J. Geochem.*, 32 (2013) 380.
19. C.W. Bale, E. Bélisle, P. Chartrand, S.A. Decterov, G. Eriksson, A.E. Gheribi, K. Hack, I.H. Jung, Y.B. Kang, J. Melançon, A.D. Pelton, S. Petersen, C. Robelin, J. Sangster and M-A. Van Ende, FactSage Thermochemical Software and Databases, 2010-2016. *Calphad*, 54 (2016) 35.
20. S. Aronson, *J. Nucl. Mater.*, 107 (1982) 343.
21. P.J. Spencer, *Thermochim. Acta*, 314 (1998) 1.
22. A. Bayón, V. A. de la Peña O'Shea, D.P. Serrano and J.M. Coronado, *Int. J. Hydrogen Energy*, 38 (2013) 13143.
23. M. Földvári, Handbook of thermogravimetric system of minerals and its use in geological practice, Ed. Geological Institute of Hungary, (2011) Budapest, Hungary.
24. B. Liu, P.S. Thomas, A.S. Ray, R.P Williams and S.W. Donne, *J. Therm. Anal. Calorim.*, 88 (2007) 177.
25. E. Adamczyk and V. Pralong, *Chem Mater.*, 29 (2017) 4645.
26. K Sada, B. Senthilkumar and P. Barpanda, *ACS Appl. Energy Mater.*, 1 (2018) 5410.

27. N. Xia, J. Zhao, C. Lai, H. Wang, S. Gao, Z. Zhang and J. Xu, *J. Appl. Electrochem.*, 47 (2017) 343.
28. X. Tan, S. Liu, Q. Guo, J. Zhang, S. Liang, M. He and J. Luo, *Int. J. Energy Res.*, 44 (2020) 1.
29. T. Brousse, M. Toupin, R. Dugas, L. Athouël, O. Crosnier and D. Bélanger, *J. Electrochem. Soc.*, 153 (2006) A2171.

© 2021 The Authors. Published by ESG (www.electrochemsci.org). This article is an open access article distributed under the terms and conditions of the Creative Commons Attribution license (<http://creativecommons.org/licenses/by/4.0/>).